Temperature Dependence of Effective Thermal Conductivity and Thermal Diffusivity of Treated and Untreated Polymer Composites

Rajni Agarwal,[1] N. S. Saxena,[1] Kanan Bala Sharma,[1] S. Thomas,[2] M. S. Sreekala[3]

[1] Condensed Matter Physics Laboratory, Department of Physics, University of Rajasthan, Jaipur 302 004, India
[2] School of Chemical Sciences, M. G. University, Kottayam 686560, Kerala, India
[3] Rubber Research Institute of India, Kottayam 686009, Kerala, India

ABSTRACT: Thermal properties, such as thermal conductivity, thermal diffusivity, and specific heat, of treated and untreated oil palm fiber–reinforced PF composites were measured simultaneously at room temperature and normal pressure using the transient plane source (TPS) technique. An increase in thermal conductivity was observed in the fiber-treated and resin-treated composites. Surface modifications of fibers by prealkali, potassium permanganate, and peroxide treatments increased the fiber–matrix adhesion by increasing porosity and pore size of the fiber surfaces. The increase in crosslinking enhanced the thermal conductivity of a composite of resin treated with peroxide compared to other composites. Also an attempt was made to explain the temperature dependence of thermal conductivity and thermal diffusivity of amorphous polymer samples using the same technique. It was observed that at the glass-transition peak of the polymer, thermal conductivity and diffusivity were maximum. Below and above this temperature their values decreased. This has been explained on the basis of predominant scattering processes. An empirical relationship was established for the theoretical prediction of thermal conductivity and diffusivity. © 2003 Wiley Periodicals, Inc. J Appl Polym Sci 89: 1708–1714, 2003

Key words: reinforced composites; thermal conductivity; thermal diffusivity; glass-transition temperature

INTRODUCTION

Natural fiber–reinforced thermoset composites have received considerable attention, as they exhibit good mechanical properties, dimensional stability, and remarkable environmental and ecological advantages. Over the past decade cellulose-based natural fibers have been preferred as a potential source for making low-cost composite materials, especially in developing tropical countries where these fibers are abundant. Natural fibers possess moderately high strength and stiffness and hence can be used as reinforcing material in polymeric resin matrices to make useful structural composite materials.[1] Lack of good interfacial adhesion and poor resistance to moisture absorption make the use of natural fiber–reinforced composites less attractive. This problem can be overcome by treating these fibers with suitable chemicals.[2]

Many studies have been reported concerning the effect of different aging conditions on the physical and mechanical properties of natural fiber–reinforced polymer composites. Treated fiber–filled thermoset composites offer good mechanical and dimensional stability under extreme conditions. Studies on composites containing natural fibers are important because of the renewable nature, low cost, and amenability to chemical modifications of these composites.

The major cash crop oil palm (*Elaesie guineesis*) originated in the tropical forests of West Africa. Now it is cultivated commercially in India and Malaysia and in some other tropical countries. One of the fillers obtained from oil palm is empty fruit bunch (OPEFB) fiber. It represents a very abundant, inexpensive renewable resource. OPEFB is obtained after the removal of oil seeds from fruit bunch for oil extraction. OPEFB fiber is extracted by the retting process.[3] The average yield of OPEFB fiber is about 400 g per bunch. These fibers must be cleaned of oily and dirty materials. When left on the plantation floor, these waste materials create great environmental problems. Therefore, economical utilization of these fibers will be beneficial.[4]

Chemical studies have shown that oil palm fiber has a high content of cellulose, which plays an important role in the fiber's performance. OPEFB fiber can be a better reinforcement in brittle plastics such as phenol–formaldehyde because it can improve the toughness of brittle plastic.[3] Before reinforcement, surface modifications of the fibers by a prealkali treatment, $KMnO_4$, and peroxide treat-

ment were carried out. Fiber became thinner upon alkali treatment. This may be because of dissolution of natural and artificial impurities on the fiber surface.

OPEFB fiber–reinforced phenol–formaldehyde composite is an effective substitute for conventional building materials. It may be used in the fabrication of doors, roofing, tiles, and so on.[3]

Reinforcement of polymer using OPEFB fiber improves desirable thermal and mechanical properties and its performance characteristics.

This article reports on an attempt to study the thermal characteristics of OPEFB fiber–reinforced composites with PF resin. The effect of fiber and resin treatments on thermal conductivity, thermal diffusivity, and specific heat were analyzed. An empirical relationship between the temperature dependence of the thermal conductivity and the thermal diffusivity of these samples was established using a least-squares parabola fit to the experimental results. The TPS method was used for this purpose.

EXPERIMENTAL

Materials and composite fabrication

The composites were prepared by reinforcing OPEFB fiber in phenol–formaldehyde resin. The resole-type phenol–formaldehyde was procured from West Coast Polymers Pvt. Ltd. (Kannur, Kerala, India). The solid content of the resin was $50 \pm 1\%$. Caustic soda was used as a catalyst during the manufacturing. The hand layup technique, followed by compression molding at 100°C for about 30 min, was adopted for composite preparation.[4]
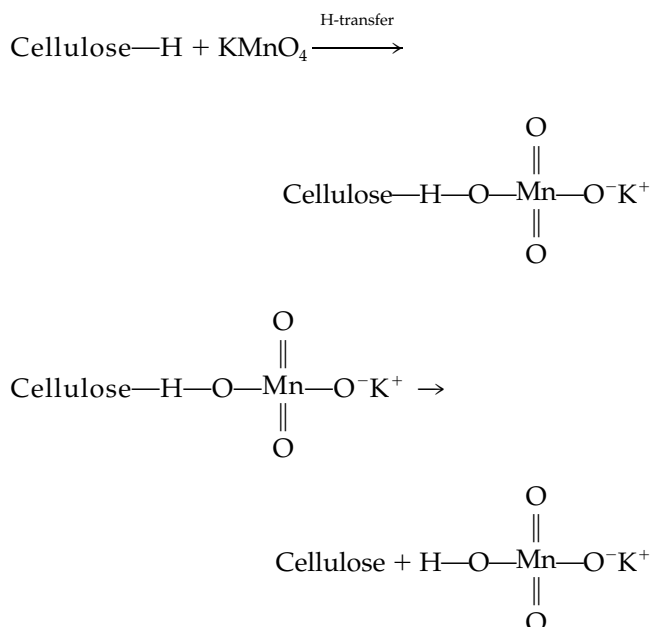
The total fiber loading of the composite was kept constant at 40 wt %, fiber length of 40 mm, and average diameter of 0.02×10^{-4} μm. The chemicals used for fiber surface modification were reagent-grade $KMnO_4$ and benzoyl peroxide.

Fiber surface modifications

Permanganate treatment (sample code 1)

Fibers were pretreated with alkali and then dipped in potassium permanganate solution in acetone for about 2–3 min. Permanganate solution concentrations of 0.01%, 0.05%, and 0.1% were used. Fibers were then washed in distilled water and finally dried. Fiber became soft and its color changed upon permanganate treatment. This treatment led to the formation of cellulose radicals through MnO_3^- ion formation. The radicals enhanced the chemical interlocking at the interface.

The reaction scheme follows:

$$\text{Cellulose—H} + KMnO_4 \xrightarrow{\text{H-transfer}}$$

$$\begin{array}{c} O \\ \parallel \\ \text{Cellulose—H—O—Mn—O}^- K^+ \\ \parallel \\ O \end{array}$$

$$\begin{array}{c} O \\ \parallel \\ \text{Cellulose—H—O—Mn—O}^- K^+ \rightarrow \\ \parallel \\ O \end{array}$$

$$\begin{array}{c} O \\ \parallel \\ \text{Cellulose} + \text{H—O—Mn—O}^- K^+ \\ \parallel \\ O \end{array}$$

Fiber peroxide treatment (sample code 2)

Fibers were coated with benzoyl peroxide from acetone solution after alkali pretreatment. A saturated solution of peroxide in acetone was used. Finally, the fibers were dried. The decomposition of the peroxide and the subsequent reaction at the interface were expected to occur at the time of curing of composites. Higher temperature was favored for decomposition of the peroxides. This can be shown as

$$RO - OR \rightarrow 2 RO^.$$

$$RO \cdot + \text{cellulose—H} \rightarrow R - OH + \text{Cellulose}.$$
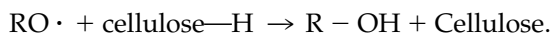
Resin peroxide treatment (Sample code 3)

PF resin was treated with benzoyl peroxide. Different quantities of the peroxide (to make concentrations of 0.1%, 0.5%, and 1.0% of the resin) were added into the resin and stirred for 1 h for intimate mixing. Peroxide can act as a free-radical initiator and can take part in crosslinking reactions.

Measurements

Thermal conductivity and thermal diffusivity of fiber-reinforced polymer composites were measured simultaneously at room temperature and normal pressure using transient plane source (TPS) technique. In this technique the source of heat is a hot disk made of a bifilar spiral that also serves as a sensor of the temperature increase in the samples. The plane disk sensor, as shown in Figure 1, was placed between two pieces of the sample material, 1.8×1.8 cm in size and 3.0 mm thick, and then heated (typical temperature
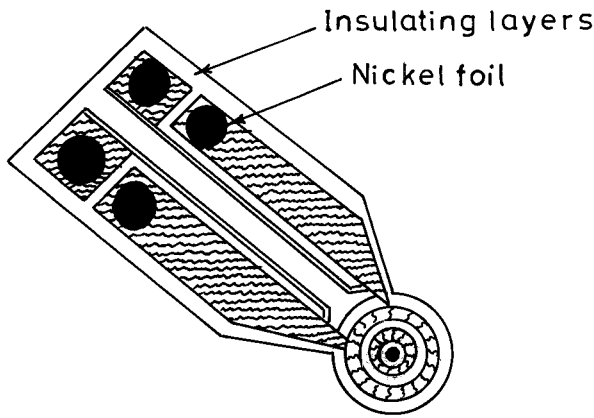
Figure 1 Hot disk sensor.

increase of 0.5–1.0 K) by an electrical current for a short time. The voltage increase over the sensor was precisely recorded.

Assuming a conducting pattern to be in the y,z plane of a coordinate system placed inside an infinite solid with a thermal conductivity, λ, a thermal diffusivity, χ, and a specific heat per unit volume, ρc the rise in temperature at a point y,z at time t from an output power per unit area Q, is given by[5,6]

$$\Delta T(y, z, t) = \frac{1}{8\pi^{3/2}\rho c} \int \frac{dt'}{[\chi(t - t')]^{3/2}}$$

$$\times \int dy' dz' Q(y', z', t') \exp\left[\frac{-(y - y')^2 - (z - z')^2}{4\chi(t - t')}\right] \tag{1}$$

where A is the total area of the conducting pattern exposed to a certain temperature increase. Equation (1) can be written in a more general form using a simple transformation of the variable t to τ, given as

$$\Delta T(y, z, \tau) = \frac{1}{4\pi^{3/2}a\lambda} \int_0^\tau \frac{d\sigma}{\sigma^2} \int_A dy' dz' Q$$

$$\times \left(y', z', t - \frac{\sigma^2 a^2}{\chi}\right) \exp\left(\frac{-(y - y')^2 - (z - z')^2}{4\sigma^2 a^2}\right) \tag{2}$$

where a is a constant (radius of hot disk) that provides a measurement of the overall size of resistive pattern and θ is known as the characteristic time.

Because of the flow of current through the sensor, the temperature increase, $\Delta T(\tau)$, gives rise to a change in the electrical resistance, $\Delta R(t)$, which is given as

$$\Delta R(t) = \alpha R_0 \overline{\Delta T(\tau)} \tag{3}$$

where R_0 is the resistance of the TPS element before initiation of the transient recording, α is the temperature coefficient of resistance (TCR), and $\Delta T(\tau)$ is the mean value of the time-dependent temperature increase of the TPS element. $\Delta T(\tau)$ is calculated by averaging the increase in temperature of the TPS element over the sampling time because the concentric ring sources in the TPS element have different radii and are placed at different temperatures during the transient recording.

According to Gustafsson[5,6]

$$\overline{\Delta T(\tau)} = \frac{P_0}{\pi^{3/2}a\lambda} D_s(\tau) \tag{4}$$

where

$$D_s(\tau) = (m(m + 1))^{-2} \int_0^\tau \frac{d\sigma}{\sigma^2}$$

$$\times \left[\sum_{l=1}^m l \sum_{j=1}^m j \cdot \exp\left(\frac{-(l^2 + j^2)}{4\sigma^2 m^2}\right) L_0\left(\frac{lj}{2\sigma^2 m^2}\right)\right] \tag{5}$$

P_0 is the total output of power, and L_0 is the modified Bessel function.

A simple bridge arrangement, as shown in Figure 2, has been used to record the potential difference variations, which normally are of the order of a few millivolts during the transient recording. Assuming that the resistance increase will cause a potential difference variation, $\Delta \underline{U}(t)$, measured by the voltmeter in the bridge, the analysis of the bridge indicated that

$$\Delta E(t) = \frac{R_s}{R_s + R_0} I_0 \Delta R(t) = \frac{R_s}{R_s + R_0} \frac{I_0 \alpha R_0 P_0}{\pi^{3/2}a\lambda} D_s(\tau) \tag{6}$$

where

$$\Delta E(t) = \Delta U(t)[1 - C \cdot \Delta U(t)]^{-1} \tag{7}$$
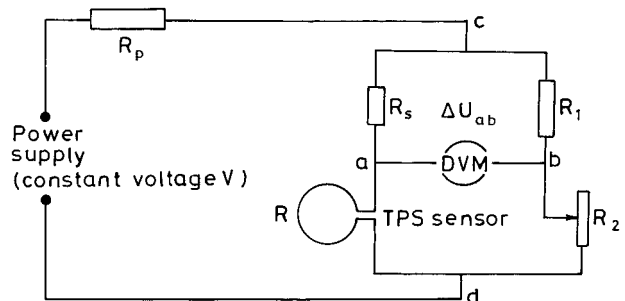
and

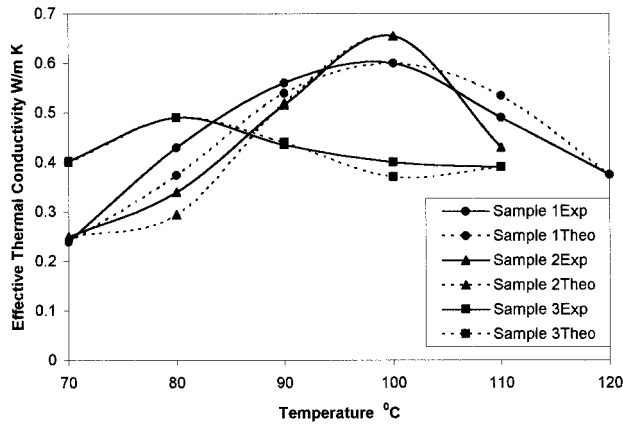**Figure 2** Schematic bridge arrangement for transient plane source.

Figure 3 Experimental and theoretical curves of temperature versus effective thermal conductivity.

$$C = \frac{1}{R_s I_0 \left[1 + \dfrac{\gamma R_p}{\gamma(R_s + R_0) + R_P} \right]} \qquad (8)$$

R_S is a standard resistance with a current rating that is much higher than I_0, which is the initial heating current through the arm of the bridge containing the TPS element; and γ is a constant that was chosen to be 100 in the present measurement.

Calculating $Ds(\tau)$ using a computer program and recording the change in potential difference, $\Delta U(t)$, the λ can be determined. Similarly, diffusivity, χ, can be determined by finding the τ values from the transient event.

The values of effective thermal conductivity and thermal diffusivity for all the treated samples, measured at different temperatures using the TPS method, were plotted (Figs. 3 and 4). It can be observed that thermal conductivity and diffusivity are nonlinear functions of temperature.

A peak was observed around 100°C for samples 1–2 and at 80°C for sample 3. Theoretical prediction of the thermal conductivity and thermal diffusivity with temperature was made by using the empirical relations:

$$\lambda = A + B(T_0 - T)^2 + D(T_0 - T)^3 \qquad (9)$$

and

$$\chi = a + b(T_0 - T)^2 + d(T_0 - T)^3 \qquad (10)$$

where A, B, D, a, b, and d are constants; T_0 is the characteristic temperature in degrees Celsius at which thermal conductivity and diffusivity of the samples become maximum.

The thermal conductivity and thermal diffusivity measurements of these samples were made in a temperature range starting at 60°C and going up to 120°C,

using the TPS technique. For high temperature measurements of this type, separate mica-covered TPS sensors are used (Fig. 1). Sensor-sandwiched sample pieces were kept in a furnace for heating the samples to the desired temperature. Before taking readings, a sample was kept in the desired temperature environment for a reasonably long time so that no temperature gradient remained in the sample. Measurements were made after reaching isothermal conditions.

Models used

Prediction of polymer composites has been made from time to time using theoretical models.[7–10] Out of these, the one proposed by Agari et al.[9] has shown the closest approximation to the experimental data over a wide range of filler contents for the composites in this study. Thermal conductivities of composites in parallel and series conductions can be estimated using the following equations, respectively:
Parallel conduction:

$$\lambda = V\lambda_2 + (1 - V)\lambda_1 \qquad (11)$$

Series conduction:

$$\frac{1}{\lambda} = \frac{V}{\lambda_2} + \frac{1 - V}{\lambda_1} \qquad (12)$$

where λ is the thermal conductivity of the composite, λ_1 is the thermal conductivity of the polymer, λ_2 is thermal conductivity of the filler, and V is the volume fraction of the filler in the composite.

$$\frac{\lambda_e - \lambda_f}{\lambda_m - \lambda_f} \left(\frac{\lambda_m}{\lambda_e} \right)^{1/3} = (1 - V) \qquad (13)$$

Another model used for calculating thermal conductivity of filler is Bruggeman's model[11,12] which is a variable dispersion equation for the concentration of
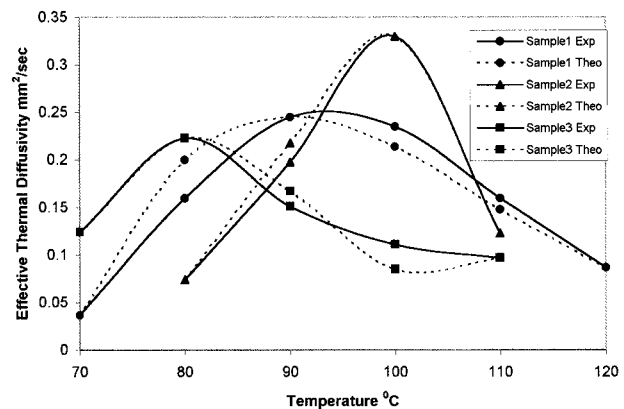

Figure 4 Experimental and theoretical curves of temperature versus effective thermal diffusivity.

TABLE I
Thermal Conductivity and Thermal Diffusivity of Filler and PF composite

Sample number	Samples	Sample size (cm)	Thermal conductivity of filler λ_f (W/mK)		Effective Thermal conductivity of PF composite λ_e (W/mK)	Effective Thermal diffusivity χ_e (mm^2/sec)
			Agari model	Bruggeman model		
1	Fiber KMnO$_4$ Treated (40 wt %)	2.0*1.8	0.4350	0.4330	0.39	0.19
2	Fiber Peroxide treated (40 wt %)	2.0*1.9	0.4590	0.4550	0.40	0.20
3	Resin Peroxide Treated (40 wt %)	2.0*2.0	0.4960	0.4890	0.41	0.18
4	Untreated (40 wt %)	1.2*1.2	0.2435	0.2413	0.29	0.16

the dispersed phase, V, a volume fraction larger than 10% or 15%, which is good in predicting the effective thermal conductivity of a dispersed composite containing a wide range of filler sizes. Here λe and λf are the thermal conductivities of the composite and the fiber, respectively and V is the volume fraction of the filler.

RESULT AND DISCUSSION

Effective thermal conductivity of all the treated and untreated PF composites was calculated using Agari's and Bruggeman models, and the result were in fair agreement. The results also showed that thermal conductivity of fillers increases after treatment and, hence, so the conductivity of the composite (Table I).

Experimental values of effective thermal conductivity and effective thermal diffusivity at room temperature of all the treated and untreated composites are given in Table I. From the table it can be clearly seen that effective thermal conductivity of the composite increased after treatments.

It is well known that a fiber surface is porous, having pores with an average diameter of 0.07 μm. Pore size and number of pores increase after prealkali treatment of the fiber, which enhances the coupling between the fiber and the matrix. Hence, effective thermal conductivity increases.

Prealkali treatment of treated samples dissolves and removes fatty acids, phenolic compounds, and their condensation products, which form the waxy cuticle layer. Loss of cuticle by the rupture of alkali-sensitive bonds leads to a rough surface. Alkali treatment increases the fiber surface adhesion characteristics by removing natural and artificial impurities, thereby increasing the thermal conductivity of the fiber as well as of the composite. Various fiber treatments such as KMnO$_4$ and peroxide treatment also increased the thermal conductivity of the fiber. This occurs because of the formation of cellulose radicals in these treatments, which enhances the chemical interlocking at the interface. Peroxide can act as a free-radical initiator and can take part in crosslinking reactions, which in turn increase dimensional stability under load and elevated temperatures. Therefore, the effective thermal conductivity of the treated samples was higher compared those that were untreated.

The thermal conductivity of the resin treated with benzoyl peroxide composite was slightly greater than the fiber-treated composites. A slight edge in the effective thermal conductivity of the resin-treated composites over the effective thermal conductivity values of the fiber-treated composites was a result of the slight difference in the chemical interlocking, which was also dependent on the polarization of the fiber in the KMnO$_4$ and peroxide treatments.

The experimental results of high-temperature studies of effective thermal conductivity and effective thermal diffusivity of all the samples tested are presented in Tables III and IV. The temperature dependence of

TABLE II
Effective Thermal Conductivity, W/mK vs Temperature

Temperature °C	Experimental			Theoretical		
	Sample 1	Sample 2	Sample 3	Sample 1	Sample 2	Sample 3
70	0.24	0.250	0.402	0.240	0.250	0.400
80	0.43	0.340	0.490	0.374	0.295	0.490
90	0.516	0.516	0.435	0.540	0.520	0.440
100	0.600	0.655	0.400	0.600	0.655	0.370
110	0.490	0.430	0.390	0.534	0.430	0.390
120	0.375	-	-	0.375	-	-

TABLE III
Effective Thermal Diffusivity, mm²/sec vs Temperature

Temperature °C	Experimental			Theoretical		
	Sample 1	Sample 2	Sample 3	Sample 1	Sample 2	Sample 3
70	0.037	-	0.124	0.037	-	0.124
80	0.160	0.074	0.223	0.200	0.074	0.223
90	0.245	0.198	0.151	0.245	0.218	0.167
100	0.235	0.330	0.111	0.214	0.330	0.085
110	0.160	0.123	0.097	0.148	0.123	0.097
120	0.087	-	-	0.087	-	-

thermal conductivity (Fig. 3) showed a gradual increase, reached a maximum, and then showed a decreasing trend for all samples. In the temperature region before and after the peak in the thermal conductivity curve, structure scattering, which is temperature independent, played an important role in the thermal resistance. In addition, this chain defect scattering and vacant site scattering, the former below the peak region and the latter after the peak, contributes to thermal resistance. These aspects are common to the amorphous polymers showing the type of temperature dependence exhibited by the samples.

Effective thermal diffusivity versus temperature plots for all the samples are presented in Figure 4. It can be seen that thermal diffusivity increased with temperature, proceeded toward a maximum, which occurred at almost the same temperature at which thermal conductivity showed its maximum or peak value. For higher temperatures, thermal diffusivity fell sharply. The trend in the variation of thermal diffusivity with the filler material was also found to be similar to the behavior of thermal conductivity.

It can be observed from Figures 3 and 4 that the agreement is reasonably good in the temperature range under consideration between the experimental results obtained with the TPS method and the results computed from the empirical eqs. (9) and (10) . Even in amorphous polymers there exists some local order, which is termed intermediate range order (IRO). In the low-temperature region ($T < T_0$), below the glass-transition peak, the temperature dependence of effective thermal conductivity and effective thermal diffusivity was controlled by variation of the phonon mean free path. During cooling certain defects also were

created in the system. Hence, below the glass-transition peak, structure scattering and chain defect scattering were the main phonon scattering mechanisms. In the former, case lattice waves propagated uniformly inside each small domain and then were abruptly scattered by a sudden change at the boundary. The dimensions of IRO at the glass-transition peak depend mainly on the processing conditions and degree of polymerization; hence, it does not vary with temperature. Therefore, the contribution to thermal resistance corresponding to these processes is temperature independent.[13,14] The first term in both empirical eqs. (9) and (10) represents the contribution to thermal resistance of structure scattering. Values of constants in equations 9 and 10 are presented in Table IV.

Chain defects[15] also scatter phonons. In the temperature region ($T < T_0$) below the glass-transition peak, with a rise in temperature, the polymeric chains straightened out more and more, increasing the corresponding mean free path, and thus the contribution to the corresponding thermal resistance decreased linearly with the rise in temperature. This increased the effective thermal conductivity of the polymer composite, and it became maximum in the vicinity of the glass-transition peak temperature.

At temperatures above the glass-transition peak region, scattering by microvoids (vacant site scattering) became predominant in addition to structure scattering. As temperature increased and the polymer passed to the rubbery state, individual units, atomic groups, and small chain segments gradually underwent intensive thermal motion and large torsional rotations, and the sliding of the chain segments started to play a dominant role in governing the variation of properties

TABLE IV
Values of constants A, B, D, a, b, d and T_0 in Equations 9 and 10 for the Effective Thermal Conductivity and Effective Thermal Diffusivity of Phenol Formaldehyde Composites

Sample	Peak value Temperature T_0(°C)	Constants for Effective Thermal Conductivity			Constants for Effective Thermal Diffusivity		
		A (W/m-K)	B (W/m-K³)	D (W/m-K⁴)	a (mm²/sec)	b (mm²/sec-K²)	d (mm²/sec-K³)
1	100	0.600	-0.63×10^{-3}	0.325×10^{-5}	0.245	-0.038×10^{-2}	-0.69×10^{-5}
2	100	0.655	-1.80×10^{-3}	4.500×10^{-5}	0.330	-0.160×10^{-2}	4.77×10^{-5}
3	80	0.490	-0.70×10^{-3}	-1.970×10^{-5}	0.223	-0.077×10^{-2}	-2.15×10^{-5}

with temperature. This had a twofold effect on the structure of the system. Initially the dominant chain movements created some vacant sites or microvoids that scattered phonons in a way similar to the point defects.[3] With the rise in temperature, the number and size of these microvoids increased, and, consequently, the contribution of vacant site scattering to thermal resistance would increase linearly with temperature. Thus, structure scattering and vacant site scattering became predominant scattering processes over a certain range of temperature above the glass-transition peak, resulting in a decrease in the thermal conductivity with a rise in temperature.

CONCLUSIONS

Results show that thermal conductivity increased after fiber and resin treatments of the composites. The fiber treatment increased the thermal conductivity of the fiber and hence of the composites to different extents depending on the fiber–matrix adhesion. Thermal conductivity was maximum for a composite in which resin was treated with peroxide. This is because of the increase in crosslinking of the polymer units.

References

1. Geethamma, V. G.; Reethamma, J.; Sabu, T. J Appl Polym Sci 1995, 55, 583.
2. Kuruvilla, J.; Sabu, T. Composites Science and Technology 1995, 53, 99.
3. Sreekala, M. S.; Sabu, T.; Neelkantan, N. R. J Polym Eng 1996, 16, 4.
4. Sreekala, M. S.; Kumaran, M. G.; Sabu, T. J Appl Polym Sci 1997, 66, 821.
5. Gustafsson, S. E. Rev Sci Instrum 1991, 62, 797.
6. Gustafsson, S. E. Rev Sci Instrum 1991, 61, 197.
7. Agari, Y.; Tanaka, M.; Nagai, S.; Uno, T. J Appl Polym Sci 1987, 34, 1429.
8. Agari, Y.; Uno, T. J Appl Polym Sci 1986, 32, 5705.
9. Agari, Y.; Veda, A.; Tanaka, M.; Nagai, S. J Appl Polym Sci 1990, 40, 929.
10. Agari, Y.; Veda, A.; Tanaka, M.; Nagai, S. J Appl Polym Sci 1991, 41, 1665.
11. Bruggeman, D. A. G. Ann Phys 1935, 24, 636.
12. Taylor, R. High Temps—High Pressure 1983, 15, 299.
13. Prepechoko, I. I. An Introduction to Polymer Physics; Mir Publishers: Moscow, 1981; Chapter 3.
14. Klemens, P. G. In Thermal Conductivity; Tye, R. P., Ed.; Academic Press: New York, 1958; Vol. 1, Chapter 1.
15. Dashora, P.; Gupta, G. Polymer 1996, 37(2), 231.